Available online at www.sciencedirect.com
ScienceDirect
Advances in Space Research 40 (2007) 1432–1440
ADVANCES IN SPACE RESEARCH (a COSPAR publication)
www.elsevier.com/locate/asr

Modeling atmosphere emission from magnetic neutron stars

Wynn C.G. Ho [a,*], Philip Chang [b], David L. Kaplan [a,1], Kaya Mori [c], Alexander Y. Potekhin [d], Matthew van Adelsberg [e]

[a] *Kavli Institute for Astrophysics and Space Research, Massachusetts Institute of Technology, Cambridge, MA 02139, USA*
[b] *Department of Astronomy, 601 Campbell Hall, University of California, Berkeley, CA 94720, USA*
[c] *Department of Astronomy and Astrophysics, University of Toronto, 50 St. George Street, Toronto, Ontario M5S3H4, Canada*
[d] *Ioffe Physico-Technical Institute, Politekhnicheskaya 26, 194021 St. Petersburg, Russia*
[e] *Center for Radiophysics and Space Research, Department of Astronomy, Cornell University, Ithaca, NY 14853, USA*

Received 2 November 2006; received in revised form 20 March 2007; accepted 3 April 2007

Abstract

Since their discovery, neutron stars have been recognized to be unique natural laboratories for helping our understanding of fundamental physics, including nuclear and particle physics and the theory of gravity. The excellent sensitivity of the new X-ray telescopes, e.g., *Chandra* and *XMM-Newton*, is ideal for the study of cooling, isolated neutron stars, which emit at these energies. In order to exploit the wealth of information contained in the data, a thorough knowledge of the emission properties of neutron stars is necessary. We describe our work on constructing atmosphere models, which determine the observed spectra from neutron stars. In particular, we discuss the effects of vacuum polarization and bound atoms on the atmosphere structure and spectra. We show that our partially ionized hydrogen atmosphere model spectra can fit the multi-wavelength spectrum of the neutron star RX J1856.5–3754. On the other hand, mid-Z element atmospheres may fit other isolated neutron stars, such as 1E 1207.4–5209.

Keywords: Magnetic fields; Radiative transfer; Stars: Atmospheres; Stars: Magnetic fields; Stars: Neutron; X-rays: Stars

1. Introduction

The observed radiation from a neutron star (NS) originates in a thin atmospheric layer (with scale height $\sim$0.1–10 cm and density $\rho \sim 0.1$–10^3 g cm^{-3}) that covers the NS surface. The properties of this atmosphere, such as its chemical composition, equation of state (EOS), and especially its radiative opacity, directly determine the characteristics of the observed spectrum. Accurate modeling of the NS atmosphere is therefore necessary to correctly interpret the observational data.

Steady progress has been made over the years in modeling NS spectra. Since the NS surface emission is thermal in nature, it has been modeled at the lowest approximation with a blackbody spectrum. While the surface composition of the NS is unknown, a great simplification arises due to the efficient gravitational separation of light and heavy elements (with timescales on the order of seconds; Alcock and Illarionov, 1980). Early works on atmospheric spectra assumed emission from light element, unmagnetized atmospheres (the latter assumption being valid for $B \lesssim 10^9$ G); computed spectra exhibit a significant deviation from a Planckian shape and distinctive hardening with respect to a blackbody (Romani, 1987; Rajagopal and Romani, 1996; Zavlin et al., 1996; Gänsicke et al., 2002).

Strong magnetic fields can significantly increase the binding energies of atoms, molecules, and other bound states (see Lai, 2001 for a review), and abundances of these bound states can be appreciable in the atmospheres of cold

* Corresponding author. Hubble Fellow. Present address: Harvard-Smithsonian Center for Astrophysics, 60 Garden Street, Cambridge, MA 02138, USA. Tel.: +1 617 496 1985; fax: +1 617 495 7356.
E-mail address: wynnho@slac.stanford.edu (W.C.G. Ho).
[1] Pappalardo Fellow.

0273-1177/$30
doi:10.1016/j.asr.2007.04.011

NSs (i.e., those with surface temperature $T \lesssim 10^6$ K; Lai and Salpeter, 1997; Potekhin et al., 1999). In addition, the presence of a magnetic field gives rise to anisotropic and polarized emission, which must be accounted for self-consistently in developing radiative transfer codes. The most comprehensive early studies of magnetic neutron star atmospheres focused on a fully ionized hydrogen plasma and moderate field strengths ($B \sim 10^{12}$–10^{13} G; Miller, 1992; Shibanov et al., 1992; Pavlov et al., 1994; Zane et al., 2000; see Pavlov et al., 1995; Zavlin and Pavlov, 2002 for a review). Despite a few seminal works (Bezchastnov et al., 1996; Bulik and Miller, 1997), only recently have self-consistent atmosphere models in the ultra-strong field ($B \gtrsim 10^{14}$ G) and relevant temperature regimes been presented (Ho and Lai, 2001; Özel, 2001; Zane et al., 2001; Lloyd, submitted for publication; van Adelsberg and Lai, 2006), and all of these rely on the assumption of a fully ionized hydrogen composition.

Modeling of NS atmospheres with more complex chemical compositions is still challenging. Magnetized heavy element atmospheres (with $B \sim 10^{12}$ G) have been studied (see Miller, 1992 for helium and mid-Z elements, where Z is the charge number; Rajagopal et al., 1997 for iron), but because of the complexity of the atomic physics and radiative transport in the presence of heavy particles and a strong magnetic field, the models were necessarily crude.

We describe here some aspects of our investigation thus far into the atmosphere and spectra of strongly magnetized NSs. We study hydrogen and mid-Z element atmospheres with magnetic fields $B \geqslant 10^{12}$ G and effective temperatures $T_{\rm eff} \gtrsim$ a few $\times 10^5$ K, so that the abundance of bound species is non-negligible. To determine the emission properties of a magnetic atmosphere, the radiative transfer equations for the two coupled photon polarization modes are solved (see Ho and Lai, 2001; Ho et al., 2003; Mori and Ho, 2007, and references therein, for details on the construction of the atmosphere models). We are able to construct self-consistent atmosphere models using the latest EOS and opacities for partially ionized hydrogen (Potekhin and Chabrier, 2003, 2004; Potekhin et al., 2004) and mid-Z elements (Mori and Hailey, 2002, 2006).

2. Vacuum polarization

In a magnetized plasma, there are two normal modes of propagation for electromagnetic waves. These are the extraordinary mode (X-mode), which is mostly polarized perpendicular to the **k**–**B** plane, and the ordinary mode (O-mode), which is mostly polarized parallel to the **k**–**B** plane, where **k** specifies the direction of photon propagation (e.g., Mészáros, 1992). It is well-known that polarization of the vacuum due to virtual e^+e^- pairs becomes significant when $B \gtrsim B_{\rm Q} = m_{\rm e}^2 c^3/e\hbar = 4.414 \times 10^{13}$ G, where $B_{\rm Q}$ is the magnetic field at which the electron cyclotron energy $\hbar\omega_{Be} = \hbar eB/m_{\rm e}c$ equals $m_{\rm e}c^2$. Vacuum polarization modifies the dielectric property of the medium and the polarization of photon modes (e.g., Adler, 1971; Tsai and Erber, 1975; Gnedin et al., 1978; Heyl and Hernquist, 1997), thereby altering the radiative scattering and absorption opacities (e.g., Mészáros and Ventura, 1979; Pavlov and Gnedin, 1984; see Mészáros, 1992 for a review). Of particular interest is the "vacuum resonance" phenomenon, which occurs when the effects of the vacuum and plasma on the linear polarization of the modes cancel each other (Gnedin et al., 1978; Mészáros and Ventura, 1979; Pavlov and Shibanov, 1979; Ventura et al., 1979). For a photon of energy E, the vacuum resonance occurs at the density

$$\rho_{\rm V} \simeq 0.964 Y_{\rm e}^{-1} (B/10^{14}\ {\rm G})^2 (E/1\ {\rm keV})^2 f^{-2}\ {\rm g\ cm^{-3}}, \qquad (1)$$

where $Y_{\rm e} = Z/A$ is the electron fraction, A is the mass number of the ion, and $f(B)$ is a slowly varying function of B (Lai and Ho, 2002; Ho and Lai, 2003). (Across the resonance, the orientation of the polarization ellipse rotates by 90°, although the helicity does not change.) For $\rho > \rho_{\rm V}$ (where the plasma effect dominates the dielectric tensor) and $\rho < \rho_{\rm V}$ (where vacuum polarization dominates), the photon modes (for $\omega \ll \omega_{Be}$) are almost linearly polarized. In this case, the X-mode and O-mode interact very differently with matter: the O-mode opacity is largely unaffected by the magnetic field, while the X-mode opacity is significantly reduced (by a factor of order ω^2/ω_{Be}^2) from the zero-field value.

Near $\rho = \rho_{\rm V}$, however, the normal modes become circularly polarized as a result of the "cancellation" of the plasma and vacuum effects. Fig. 1 shows the photon polarization ellipticities $K_\pm$ and the refractive indices $n_\pm = ck_\pm/\omega$ for the two modes as a function of density near the vacuum resonance for $B = 10^{14}$ G, $E = 1$ keV, and $\theta_B = 45°$ is the angle between **k** and **B**. The plus-mode (minus-mode)

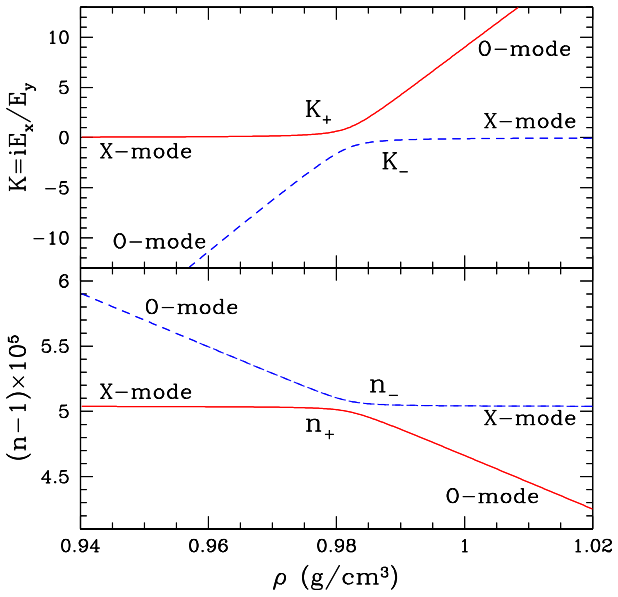

Fig. 1. Polarization ellipticities K_j (upper panel) and refractive indices n_j (lower panel) of the photon modes as functions of density near the vacuum resonance for $B = 10^{14}$ G, $\theta_B = 45°$, $E = 1$ keV, and $Y_{\rm e} = 1$.

manifests as the O-mode (X-mode) at high densities but becomes the X-mode (O-mode) at low densities. If the density variation is sufficiently gentle (see Lai and Ho, 2002), an O-mode photon created at high densities will remain on the K_+-trajectory as it travels outward and will adiabatically convert into the X-mode after traversing the resonance density.

Because the two photon modes possess very different opacities, the vacuum polarization-induced mode conversion can significantly affect radiative transfer in magnetized atmospheres. When vacuum polarization is taken into account, the photosphere densities of the two modes can be altered, depending on the location of the vacuum resonance ρ_V relative to the photosphere densities (see Fig. 2). For "normal" magnetic fields,

$$B < B_l \approx 6.6 \times 10^{13} (T/10^6\ \mathrm{K})^{-1/8} (E/1\ \mathrm{keV})^{-1/4} f^{-1/4}\ \mathrm{G}, \quad (2)$$

the vacuum resonance lies outside both photospheres (Lai and Ho, 2003a; Ho and Lai, 2004); in this case, there is no net change in the total emission spectrum. We note, however, that the X-ray polarization signals are dramatically affected by vacuum polarization in this "normal" field regime (see Lai and Ho, 2003b). For $(B/B_l)^4 \gg 1$, the O-mode photosphere is unchanged by vacuum polarization, while the X-mode photons (which carry the bulk of the flux) emerge from the vacuum resonance layers; we thus expect that the total spectrum will be affected by vacuum

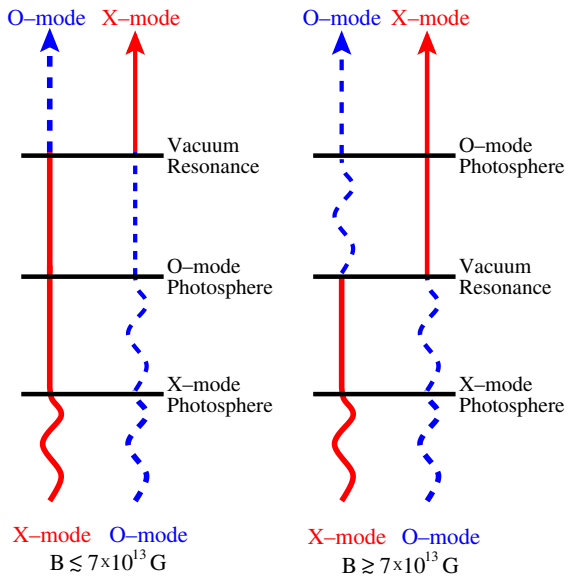

Fig. 2. Schematic diagram illustrating how vacuum polarization-induced mode conversion affects the emergent radiation from a magnetized NS atmosphere. The photosphere is defined by where the optical depth (measured from the surface) is 2/3 and is where the photon decouples from the matter. The left side applies to the "normal" field regime [$B \lesssim 7 \times 10^{13}$ G; see Eq. (2)], in which the vacuum resonance lies outside the photospheres of the two modes. The right side applies to the "superstrong" field regime ($B \gtrsim 7 \times 10^{13}$ G), in which the vacuum resonance lies between the two photospheres.

polarization in this regime. This is illustrated in Fig. 3, which shows fully ionized hydrogen atmosphere spectra with $B = 5 \times 10^{14}$ G and $T_{\rm eff} = 5 \times 10^6$ K; the curves illustrate the effect of including ("partial conv") or ignoring vacuum polarization effects (see van Adelsberg and Lai, 2006). It is clear that vacuum polarization can suppress spectral features and makes these features difficult to observe with current X-ray detectors (see, e.g., Patel et al., 2001, 2003; Juett et al., 2002; Tiengo et al., 2002; Morii et al., 2003).

3. Neutron star atmosphere models

3.1. Partially ionized hydrogen atmospheres

Previous works that attempted to fit the spectra of isolated neutron stars (INSs) with magnetic hydrogen atmosphere models assume the hydrogen is fully ionized. The temperature obtained using these models (or simple blackbodies) are in the range $kT^\infty \approx 40$–100 eV, where $T^\infty = T_{\rm eff}/(1+z_g)$, the gravitational redshift z_g is given by $(1+z_g) = (1-2GM/Rc^2)^{-1/2}$, and M and R are the mass and radius of the NS, respectively. Contrast this with the atomic hydrogen binding energies of 160 eV and 310 eV at $B = 10^{12}$ G and 10^{13} G, respectively. Therefore the atmospheric plasma should be partially ionized.

Fig. 4 illustrates the spectral differences between a fully ionized and a partially ionized hydrogen atmosphere. The atomic fraction is $\lesssim 10\%$ throughout the atmosphere. Besides the proton cyclotron line at $E_{Bp} = 6.3(B/10^{12}\ \mathrm{G})$ eV, the other features are due to bound-bound and bound-free transitions (see Potekhin and Chabrier, 2003; Ho et al., 2003). In addition, the effect of

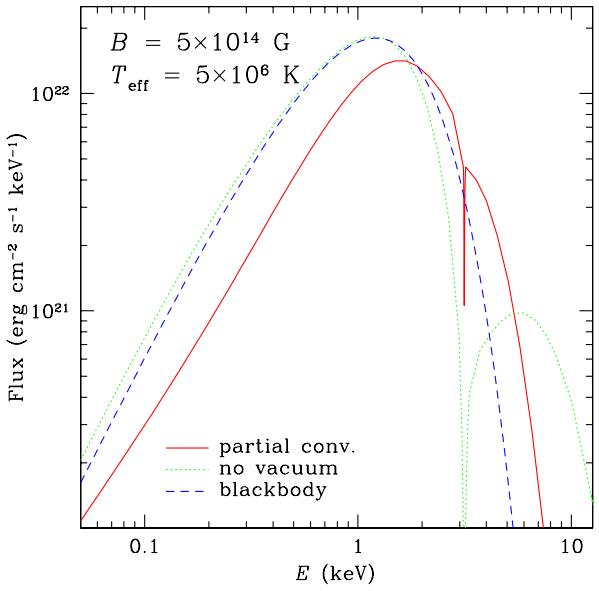

Fig. 3. Spectra of fully ionized hydrogen atmospheres with $B = 5 \times 10^{14}$ G and $T_{\rm eff} = 5 \times 10^6$ K. The solid and dotted lines are the atmospheres with and without vacuum polarization, respectively, and the dashed line is for a blackbody with $T = 5 \times 10^6$ K.

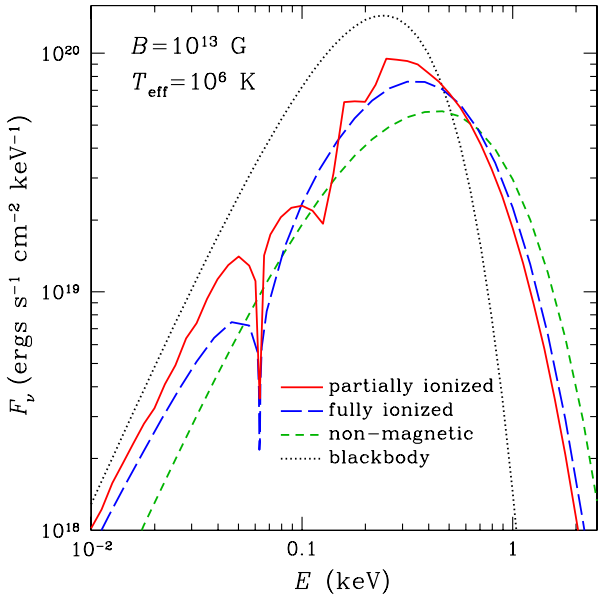

Fig. 4. Spectra of hydrogen atmospheres with $B = 10^{13}$ G and $T_{\rm eff} = 10^6$ K. The solid line is for a partially ionized atmosphere, the long-dashed line is for a fully ionized atmosphere, the short-dashed line is for a fully ionized non-magnetic atmosphere, and the dotted line is for a blackbody with $T = T_{\rm eff}$.

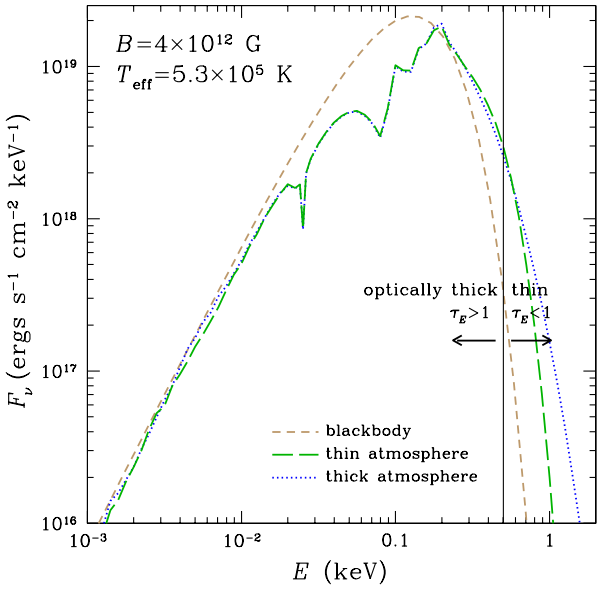

Fig. 5. Spectra of hydrogen atmospheres with $B = 4 \times 10^{12}$ G and $T_{\rm eff} = 5.3 \times 10^5$ K. The dotted and long-dashed lines are the model spectra using the "thick" atmosphere and "thin" atmosphere with an atmosphere column $y_{\rm H} = 1.2$ g cm^{-2}, respectively. The short-dashed line is for a blackbody with the same temperature. The vertical line separates the energy ranges where the atmosphere is optically thin ($\tau_E < 1$) and optically thick ($\tau_E > 1$).

bound species on the temperature profile of the atmosphere and the continuum flux is significant; thus fitting observed spectra with partially ionized models would yield different results than if fully ionized models are used.

3.2. Thin atmospheres

Conventional NS atmosphere models assume the atmosphere is geometrically thick enough so that it is optically thick at all photon energies ($\tau_E \gg 1$ for all energies E); thus the observed photons are all created within the atmosphere layer. The input spectrum (usually taken to be a blackbody) at the bottom of the atmosphere is not particularly important in determining the spectrum seen above the atmosphere since photons produced at this innermost layer undergo many absorptions/emissions. The observed spectrum is determined by the temperature profile and opacities of the atmosphere. For example, atmosphere spectra are harder than a blackbody (at the same temperature) at high energies as a result of the non-grey opacities (see Fig. 4); the opacities decline with energy so that high-energy photons emerge from deeper, hotter layers in the atmosphere than low energy photons.

However, a complication in fitting observational data of some INSs with hydrogen atmosphere models is that the model spectra are too hard at high energies. A possible mechansim for "suppressing" the high-energy emission is to consider an atmosphere that is geometrically thinner than described above, such that the atmosphere is optically thin at high energies but is still optically thick at low energies ($\tau_E < 1$ for $E > E_{\rm thin}$ and $\tau_E > 1$ for $E < E_{\rm thin}$). Thus photons with energies $E > E_{\rm thin}$ pass through the atmosphere without much attenuation (note that their contribution to thermal balance is small if most of the energy is emitted at $E < E_{\rm thin}$). If the innermost atmosphere layer (at temperature $T_{\rm thin}$) emits as a blackbody, then the observed spectrum at $E < E_{\rm thin}$ will just be a blackbody spectrum at temperature $T = T_{\rm thin}$. Motch et al. (2003) showed that a "thin" atmosphere can yield a softer high-energy spectrum than a "thick" atmosphere and used a thin atmosphere spectrum to fit the observations of RX J0720.4–3125 (see also Section 4).

3.3. Condensed iron versus blackbody emission

In addition to atmosphere models in which the deepest layer of the atmosphere is assumed to be a blackbody, we construct (more realistic and self-consistent) models in which this layer undergoes a transition from a gaseous atmosphere to a condensed surface. A surface composed of iron is a likely end-product of NS formation, and Fe condenses at $\rho \approx 561\ AZ^{-3/5}\ (B/10^{12}\ {\rm G})^{6/5}$ g cm^{-3} and $T \lesssim 10^{5.5} (B/10^{12}\ {\rm G})^{2/5}$ K (Lai, 2001); note that there is several tens of percent uncertainty in the condensation temperature (Medin & Lai, private communication; see also Medin & Lai, 2006a,b). Hydrogen condenses at $T \sim 2 \times 10^4 B_{12}^{0.65}$ K and thus requires much lower temperatures. The condensed matter surface possesses different emission properties than a pure blackbody (Brinkmann, 1980; Turolla et al., 2004; van Adelsberg et al., 2005; Pérez-Azorín et al., 2005); in particular, features can appear at the plasma and proton cyclotron frequencies.

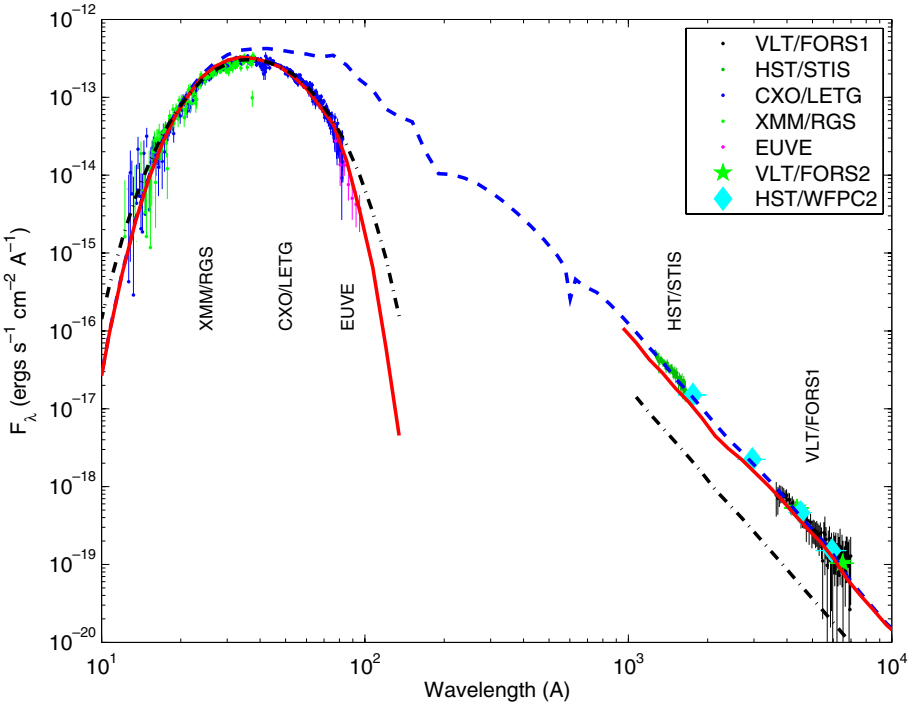

Fig. 6. Spectrum of RX J1856.5–3754 from optical to X-ray wavelengths. The data points are observations taken from various sources. Error bars are one-sigma uncertainties. Optical spectra are binned for clarity: STIS data into 30 bins at a resolution of 12 Å and VLT data into 60 bins at 55 Å resolution. The solid line is the absorbed (and redshifted by $z_g = 0.22$) atmosphere model spectrum with $B = 4 \times 10^{12}$ G, $y_H = 1.2$ g cm^{-2}, $T^\infty = 4.3 \times 10^5$ K, and $R^\infty = 17$ km. The dashed line is the unabsorbed atmosphere model spectrum. The dash-dotted line is the (absorbed) blackbody fit to the X-ray spectrum with $R^\infty = 5$ km. Note that our atmosphere model underpredicts the optical flux by 15%; however the observational and model uncertainties at these wavelengths is ~20%.

When considering thin atmospheres, we use the calculations of van Adelsberg et al. (2005) to determine the input spectrum in our radiative transfer calculations. We see from Fig. 5 that the harder spectrum at high energies in the "thick" atmosphere becomes much softer in the "thin" atmosphere and takes on a blackbody shape. In contrast, there is a negligible difference where the atmosphere is optically thick.

4. RX J1856.5–3754

4.1. Multi-wavelength spectrum of RX J1856.5–3754

In this section, we describe our work in fitting the multi-wavelength spectrum of the puzzling INS RX J1856.5–3754 (see Ho et al., 2007 for details). Single temperature blackbody fits to the X-ray spectra underpredict the optical flux by a factor of ~6–7 (see Fig. 6). X-ray and optical/UV data can best be fit by two-temperature blackbody models with $kT_X^\infty = 63$ eV, emission size $R_X^\infty = 5.1(d/140\ \mathrm{pc})$ km,[2] $kT_{opt}^\infty = 26$ eV, and $R_{opt}^\infty = 21.2(d/140\ \mathrm{pc})$ km (Burwitz et al., 2001, 2003; van Kerkwijk and Kulkarni, 2001; Braje and Romani, 2002; Drake et al., 2002; Pons et al., 2002; see also Pavlov et al., 2002; Trümper et al., 2004), where $R^\infty = R^{em}(1 + z_g)$ and R^{em} is the physical size of the emission region. However, the non-detection until recently of X-ray pulsations (down to the 1.3% level) puts severe constraints on such two-temperature models (Drake et al., 2002; Ransom et al., 2002; Burwitz et al., 2003), although it is possible that the magnetic axis is aligned with the spin axis or the hot magnetic pole does not cross our line of sight (Braje and Romani, 2002). With the very recent discovery of ~1% pulsations (Tiengo and Mereghetti, 2007), comparisons of the light curves to models has provided constraints on the geometry (Ho, 2007, submitted for publication).

Even though blackbody spectra fit the data, one expects NSs to possess atmospheres. The lack of any significant spectral features in the X-ray spectrum argues against a heavy element atmosphere (Burwitz et al., 2001, 2003), whereas single temperature hydrogen atmosphere fits overpredict the optical flux by a factor of ~100 (Pavlov et al., 1996; Pons et al., 2002; Burwitz et al., 2003). However, these previous hydrogen atmosphere results are derived using non-magnetic atmosphere models. Only a few magnetic (fully ionized) hydrogen or iron atmospheres have been considered (e.g., Burwitz et al., 2001, 2003), and even these models are not adequate, as described in Section 3.1.

[2] The most recent determination of the distance to RX J1856.5–3754 is ≈160 pc (Kaplan et al., in preparation). However, the uncertainties in this determination are still being examined. Therefore, we continue to use the previous estimate of 140(±40) pc from Kaplan et al. (2002) since the uncertainty in this previous value encompasses both the alternative estimate of 120 pc from Walter and Lattimer (2002) and the new value.

In Ho et al. (2007), we fit the multi-wavelength spectrum of RX J1856.5–3754 with our partially ionized hydrogen atmosphere models and condensed matter in strong magnetic fields (see Section 3). Fig. 6 shows that our single temperature atmosphere model can fit the entire spectrum just as well as the two-temperature blackbody models and without the large overprediction of optical/UV flux obtained by fully ionized magnetic and non-magnetic hydrogen atmosphere models. The best-fit atmosphere parameters are given in Table 1, as well as the best-fit blackbody parameters. In particular, note our more realistic NS radius $R^{\infty} \approx 17$ km compared to the blackbody radii $R^{\infty}_{\rm X} \approx 5$ km and $R^{\infty}_{\rm opt} = 21$ km.

4.2. Creation of thin hydrogen atmospheres

The atmosphere model fit above gives an atmosphere column $y_{\rm H} \approx 1$–$2\ {\rm g\ cm^{-2}}$. A hydrogen atmosphere with this column density has a total mass of $M_{\rm H} \approx 1 \times 10^{13}\ (R/10\ {\rm km})^2\ (y_{\rm H}/1\ {\rm g\ cm^{-2}})$ g or about 10^{-21} of the mass of a $1.4 M_{\odot}$ NS. Since the diffusion timescale is extremely short in a high gravity environment (Alcock and Illarionov, 1980), the atmosphere contains the bulk of the total hydrogen budget of the NS. The origin of such thin H layers is a problem which we now address by briefly discussing possible mechanisms for generating thin H atmospheres. We leave a more detailed study to future work.

Accretion at low rates may create a thin hydrogen layer on the NS surface. A thin hydrogen layer of $y_{\rm H} = 1\ {\rm g\ cm^{-2}}$ has a total mass of $\approx 6 \times 10^{-21}\ M_{\odot}$. Hence the time-averaged accretion rate over the age of RX J1856.5–3754 ($\sim 5 \times 10^5$ yr; Walter and Lattimer, 2002; Kaplan et al., 2002) is $\approx 0.8\ {\rm g\ s^{-1}}$. For the case of RX J0720.4 − 3125 with $y_{\rm H} = 0.16\ {\rm g\ cm^{-2}}$, such a mass layer may result if the time-averaged accretion rate onto the NS is about $0.06\ {\rm g\ s^{-1}}$ over 10^6 yr (Motch et al., 2003). Such small amounts of accretion indicate an enormous fine-tuning problem. Thus this process is unlikely to be the origin of the thin hydrogen envelope.

Table 1
Fits to the X-ray data of RX J1856.5–3754

	Atmosphere	Blackbody
Model parameters		
$B\ (10^{12}{\rm G})$	4	
$y_{\rm H}\ ({\rm g\ cm^{-2}})$	1.2	
Fit results		
$N_{\rm H}\ (10^{20}\ {\rm cm^{-2}})$	1.30(2)	0.91(1)
$T^{\infty}\ (10^5\ {\rm K})$	4.34(2)	7.36(1)
$R^{\infty}\ (d_{140}\ {\rm km})$	17	5.0
z_g	0.22(2)	
$\chi^2_{\rm r}/{\rm dof}$	0.86/4268	0.86/4269

Numbers in parentheses are 68% confidence limits in the last digit(s). The formal fit uncertainty for $R^{\infty} < 10\%$; however, since the radius determination depends on the distance, we conservatively adopt the current ~30% distance uncertainty as our radius uncertainty.

We next consider the possibility that the thin hydrogen layer is a remnant from the formation of the NS. In this case, Chang and Bildsten (2003, 2004) point out that diffusive nuclear burning (DNB) is the dominant process for determining what happens to hydrogen on the surface of a NS. Due to the power law dependence of the column lifetime $\tau_{\rm col}$ on $y_{\rm H}$, DNB leaves a thin layer of hydrogen, whose thickness depends on the thermal history of the NS and the underlying composition. We find the column lifetime from a full numerical solution to be $\tau_{\rm col} \approx 10^{10}$ yr for a magnetized envelope with $B = 10^{12}$ G and $\tau_{\rm col} \approx 10^8$ yr for $B = 10^{13}$ G (assuming $M = 1.4\ M_{\odot}$, $R = 14$ km, $T_{\rm eff} = 5 \times 10^5$ K, and $y_{\rm H} = 1\ {\rm g\ cm^{-2}}$). The shorter column lifetime for higher magnetic fields is due to the effect of the magnetic field on the electron equation of state, which increases the hydrogen number density in the burning layer (Chang et al., 2004). Thus there is insufficient time at the current effective temperature to reduce the surface hydrogen to such a thin column, assuming that the age of RX J1856.5–3754 is $\sim 5 \times 10^5$ yr. However, DNB was much more effective in the past when the NS was hotter. In fact, during the early cooling history of the NS, DNB would have rapidly consumed all the hydrogen on the surface (Chang and Bildsten, 2004). This leads to another fine-tuning problem: if we fix the lifetime of an envelope to some value representing the time the NS spends at a particular temperature, we find that the resulting column scales like $y_{\rm H} \propto T_{\rm eff}^{-40}$ (Chang and Bildsten, 2003); therefore, the size of the atmosphere is extremely sensitive to the early cooling history of the NS. As a result, DNB appears to be a less likely mechanism for producing such thin atmospheres.

Finally, we briefly examine a self-regulating mechanism that is driven by magnetospheric currents and may produce thin hydrogen columns on the surface. Since the accelerating potential could be as high as 10 TeV (Arons, 1984), high energy particles would create electromagnetic cascades on impact with the surface (Cheng and Ruderman, 1977). These cascades result in e/γ dissociation of surface material, analogous to proton spallation of CNO elements in accreting systems (Bildsten et al., 1992). Protons would be one of the products of this dissociation and would rise to the surface due to the rapid diffusion timescale. Since protons cannot further dissociate into stable nuclei, a hydrogen layer is built up to a column roughly given by the radiation length of the ultrarelativistic electrons, beyond which hydrogen can no longer be produced and the above mechanism terminates. The radiation length of ultrarelativistic electrons depends on the stopping physics. In the zero magnetic field limit, the stopping physics is dominated by relativistic bremsstrahlung, and the cross-section is $\sigma \sim \alpha_{\rm F} Z^2 r_0^2$, where $\alpha_{\rm F} \equiv e^2/\hbar c$ is the fine structure constant, Z is the charge number of the nuclei, and $r_0 = e^2/m_{\rm e}c^2$ is the classical electron radius (Bethe and Heitler, 1934; Heitler, 1954). This gives a stopping column $y_{\rm stop} \sim 3000\ {\rm g\ cm^{-2}}$ for hydrogen. Bethe and Ashkin (1953) and Tsai (1974) give a more accurate value,

$y_{\rm stop} \sim 60\ {\rm g\ cm^{-2}}$, for the stopping column of atomic hydrogen; thus it appears that the resulting columns are too thick. However, for sufficiently strong magnetic fields, the stopping physics of ultrarelativistic electrons is significantly modified, and the dominant stopping mechanism is via magneto-Coulomb interactions (Kotov and Kel'ner, 1985; see also Kotov et al., 1986). In magneto-Coulomb stopping, relativistic electrons traveling along field lines are kicked up to excited Landau levels via collisions and de-excite, radiating photons with energy $\gamma\hbar\omega_B$, where $\hbar\omega_B$ is the Landau cyclotron energy and γ is the Lorentz factor of the incoming electron. Compared to zero-field relativistic bremsstrahlung, the magneto-Coulomb radiation length is smaller by a factor of $\sim\pi\alpha_{\rm F}$ (Kotov and Kel'ner, 1985). Applying the correction to the Bethe and Ashkin (1953) result ($y_{\rm stop} \sim 60\ {\rm g\ cm^{-2}}$), we find this gives roughly the required thin atmosphere column, $y_{\rm stop} \sim 1\ {\rm g\ cm^{-2}}$. Though extremely suggestive, this mechanism requires a more complete study and is the subject of future work (see, e.g., Thompson and Beloborodov, 2005; Beloborodov and Thompson, 2007).

5. Mid-Z element atmospheres

Recent observations by *Chandra* and *XMM-Newton* detected spectral features from other INSs; a single or multiple absorption features were found (Haberl et al., 2003, 2004; van Kerkwijk et al., 2004; Schwope et al., 2005; Zane et al., 2005; Haberl, in press) and two broad absorption features were detected from 1E 1207.4−5209 (Sanwal et al., 2002; Mereghetti et al., 2002; Mori et al., 2005). In fact, 1E 1207.4–5209 is unique among these INSs since one of the features appears above 1 keV, while the other INSs have absorption features at $E \simeq 0.2$–0.7 keV.

Even though the NS surface composition is thought to more likely be composed of hydrogen, hydrogen atmospheres cannot produce strong spectral features at $E \gtrsim 1$ keV because (1) the binding energy of a hydrogen atom never exceeds ~1 keV at any B-field (Lai, 2001; Sanwal et al., 2002), (2) QED effects significantly reduce line strengths at $B \gtrsim 7\times10^{13}$ G (see Section 2), and (3) the fraction of hydrogen molecular ions (which may have transition lines above 1 keV; Turbiner and López, 2004) is negligible (Potekhin and Chabrier, 2004). Therefore, spectral features at $\gtrsim 1$ keV (such as the 1.4 keV absorption line of 1E 1207.4–5209) suggest a non-hydrogenic element atmosphere on the NS surface (Sanwal et al., 2002; Hailey and Mori, 2002; Mori and Hailey, 2006). Also, theoretical studies suggest that a hydrogen layer on the surface may be quickly depleted by diffuse nuclear burning or pulsar winds, thus exposing the heavier elements that lie underneath (Chang and Bildsten, 2004; Chang et al., 2004; see Section 4.2). Therefore, we have undertaken to building NS atmospheres composed of mid-Z elements, in particular carbon, oxygen, and neon; details are contained in Mori and Ho (2007). In contrast to hydrogen opacities, mid-Z element opacities are dominated by numerous bound transitions; consequently temperature profiles are closer to grey profiles and spectra are softer than hydrogen spectra and close to blackbody spectra. An example is shown in Fig. 7. The mid-Z element spectra are even softer than blackbody in the Wien tail due to photo-absorption edges (at ~1.5–2 keV for 10^{12} G). At higher energy, the spectra become harder in order to maintain radiative equilibrium. A similar feature is seen in the magnetized iron atmosphere models of Rajagopal et al. (1997). This appears to be a common signature of heavy element atmospheres. Using the results of Mori and Ho (2007), we will fit the observations of 1E 1207.4–5209 and several other INSs.

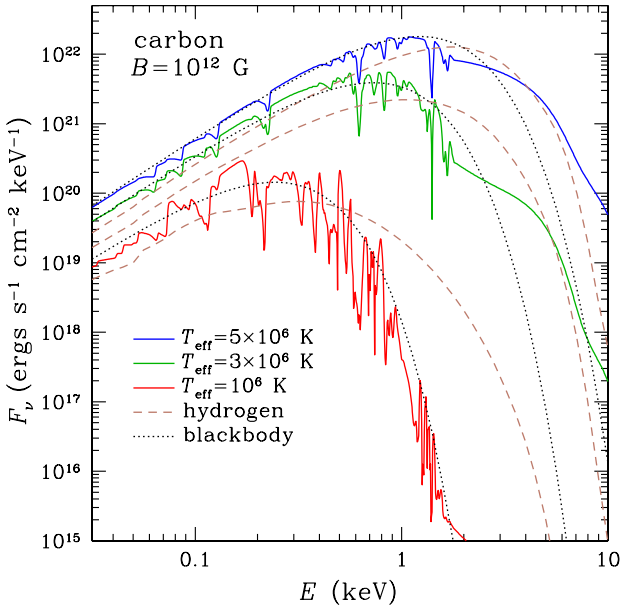

Fig. 7. Spectra of carbon atmospheres with $B = 10^{12}$ G and effective temperatures $T_{\rm eff} = 1$, 3, and 5×10^6 K. The dashed lines show hydrogen atmosphere spectra with the same B and $T_{\rm eff}$, and the dotted lines show blackbody spectra with $T = T_{\rm eff}$.

In summary, we discussed our continuing work on understanding the emission processes of NS atmospheres. We find that vacuum polarization and the presence of bound species in hydrogen and mid-Z elements can strongly influence the interpretation of observations of NSs made by modern and future spacecraft, such as *Chandra* and *XMM-Newton*.

Acknowledgements

W.H. is partially supported by NASA through Hubble Fellowship Grant HF-01161.01-A awarded by STScI, which is operated by AURA, Inc., for NASA, under contract NAS 5-26555. A.P. is partially supported by FASI Grant NSh-9879.2006.2 and RFBR Grants 05-02-16245 and 05-02-22003.

References

Adler, S.L. Photon splitting and photon dispersion in a strong magnetic field. Ann. Phys. 67, 599–647, 1971.

Alcock, C., Illarionov, A. Surface chemistry of stars I. Diffusion of heavy ions in white dwarf envelopes. ApJ 235, 534–553, 1980.

Arons, J. Magnetospheric structure and high-energy photon emission of radio pulsars. Adv. Sp. Res. 3, 287–296, 1984.

Beloborodov, A.M., Thompson, C. Corona of magnetars. ApJ 657, 967–993, 2007.

Bethe, H., Ashkin, J., in: Segrè, E. (Ed.), Experimental Nuclear Physics. Wiley, New York, p. 166, 1953.

Bethe, H., Heitler, W. On the stopping of fast particles and on the creation of positive electrons. Proc. R. Soc. A 146, 83–112, 1934.

Bezchastnov, V.G., Pavlov, G.G., Shibanov, Yu.A., Zavlin, V.E. Radiative opacities and photosphere models for soft gamma repeaters, in: Kouveliotou, C., Briggs, M.F., Fishman, G.J. (Eds.), AIP Conferer-ence Proceedings 384, Gamma-Ray Bursts. AIP, Woodbury, pp. 907–911, 1996.

Bildsten, L., Salpeter, E.E., Wasserman, I. The fate of accreted CNO elements in neutron star atmospheres – X-ray bursts and gamma-ray lines. ApJ 384, 143–176, 1992.

Braje, T.M., Romani, R.W. RX J1856–3754: Evidence for a stiff equation of state. ApJ 580, 1043–1047, 2002.

Brinkmann, W. Thermal radiation from highly magnetized neutron stars. A&A 82, 352–361, 1980.

Bulik, T., Miller, M.C. Spectral effects of the vacuum resonance in soft gamma-ray repeaters. MNRAS 288, 596–608, 1997.

Burwitz, V., Zavlin, V.E., Neuhäuser, R., Predehl, P., Trümper, J., Brinkman, A.C. Chandra LETGS high resolution X-ray spectrum of the isolated neutron star RX J1856.5–3754. A&A 379, L35–L38, 2001.

Burwitz, V., Haberl, F., Neuhäuser, R., Predehl, P., Trümper, J., Zavlin, V.E. Thermal radiation of the isolated neutron star RX J1856.5–3754 observed with Chandra and XMM-Newton. A&A 399, 1109–1114, 2003.

Chang, P., Bildsten, L. Diffusive nuclear burning in neutron star envelopes. ApJ 585, 464–474, 2003.

Chang, P., Bildsten, L. Evolution of young neutron star envelopes. ApJ 605, 830–839, 2004.

Chang, P., Arras, P., Bildsten, L. Hydrogen burning on magnetar surfaces. ApJL 616, L147–L150, 2004.

Cheng, A.F., Ruderman, M.A. Pair-production discharges above pulsar polar caps. ApJ 214, 598–606, 1977.

Drake, J.J. et al. Is RX J1856.5–3754 a quark star?. ApJ 572 996–1001, 2002.

Gänsicke, B.T., Braje, T.M., Romani, R.W. Thermal emission from low-field neutron stars. A&A 386, 1001–1008, 2002.

Gnedin, Yu.N., Pavlov, G.G., Shibanov, Yu.A. Effect of vacuum birefringence in a magnetic field on the polarization and beaming of X-ray pulsars. Sov. Astron. Lett. 4, 117–119, 1978.

Haberl, F., Magnificent seven: Magnetic fields and surface temperature distributions. Ap&SS, in press (astro-ph/0609066).

Haberl, F., Schwope, A.D., Hambaryan, V., Hasinger, G., Motch, C. Broad absorption feature in the X-ray spectrum of the isolated neutron star RBS 1223 (1RXS J130848.6+212708). A&A 403, L19–L23, 2003.

Haberl, F., Zavlin, V.E., Trümper, J., Burwitz, V. Phase-dependent absorption line in the spectrum of the X-ray pulsar RX J0720.4–3125. A&A 419, 1077–1085, 2004.

Hailey, C.J., Mori, K. Evidence of a mid-atomic number atmosphere in the neutron star 1E 1207.4–5209. ApJL 578, L133–L136, 2002.

Heitler, W. Quantum Theory of Radiation, third ed Oxford University Press, London, 1954.

Heyl, J.S., Hernquist, L. Birefringence and dichroism of the QED vacuum. J. Phys. A 30, 6485–6492, 1997.

Ho, W.C.G. Constraining the geometry of the neutron star RX J1856.5–3754. MNRAS, submitted for publication, 2007.

Ho, W.C.G., Lai, D. Atmospheres and spectra of strongly magnetized neutron stars. MNRAS 327, 1081–1096, 2001.

Ho, W.C.G., Lai, D. Atmospheres and spectra of strongly magnetized neutron stars – II. The effect of vacuum polarization. MNRAS 338, 233–252, 2003.

Ho, W.C.G., Lai, D. Spectral features in the thermal emission from isolated neutron stars: dependence on magnetic field strengths. ApJ 607, 420–425, 2004.

Ho, W.C.G., Lai, D., Potekhin, A.Y., Chabrier, G. Atmospheres and spectra of strongly magnetized neutron stars – III. Partially ionized hydrogen models. ApJ 599, 1293–1301, 2003.

Ho, W.C.G., Kaplan, D.L., Chang, P., van Adelsberg, M., Potekhin, A.Y. Magnetic hydrogen atmosphere models and the neutron star RX J1856.5–3754. MNRAS 375, 821–830, 2007.

Juett, A.M., Marshall, H.L., Chakrabarty, D., Schulz, N.S. Chandra high-resolution spectrum of the anomalous X-ray pulsar 4U 0142+;61. ApJL 568, L31–L34, 2002.

Kaplan, D.L., van Kerkwijk, M.H., Anderson, J. Parallax and proper motion of RX J1856.5–3754 revisited. ApJ 571, 447–457, 2002.

Kotov, Yu.D., Kel'ner, S.R. Magneto-Coulomb radiation of ultrarelativistic electrons in a strong magnetic field. Sov. Astron. Lett. 11, 392–394, 1985.

Kotov, Yu.D., Kel'ner, S.R., Bogovalov, S.V. Radiation by ultrarelativistic electrons entering a dense medium in a strong magnetic field. Sov. Astron. Lett. 12, 168–171, 1986.

Lai, D. Matter in strong magnetic fields. Rev. Mod. Phys. 73, 629–662, 2001.

Lai, D., Ho, W.C.G. Resonant conversion of photon modes due to vacuum polarization in a magnetized plasma: implications for X-ray emission from magnetars. ApJ 566, 373–377, 2002.

Lai, D., Ho, W.C.G. Transfer of polarized radiation in strongly magnetized plasmas and thermal emission from magnetars: effect of vacuum polarization. ApJ 588, 962–974, 2003a.

Lai, D., Ho, W.C.G. Polarized X-ray emission from magnetized neutron stars: signature of strong-field vacuum polarization. Phys. Rev. Lett. 91, 071101-1-4, 2003b.

Lai, D., Salpeter, E.E. Hydrogen phases on the surfaces of a strongly magnetized neutron star. ApJ 491, 270–285, 1997.

Lloyd, D.A. Model atmospheres and thermal spectra of magnetized neutron stars. MNRAS, submitted for publication (astro-ph/0303561).

Medin, Z., Lai, D. Density-functional-theory calculations of matter in strong magnetic fields: I. Atoms and molecules. Phys. Rev. A 74, 062507-1-14, 2006a.

Medin, Z., Lai, D. Density-functional-theory calculations of matter in strong magnetic fields: II. Infinite chains and condensed matter. Phys. Rev. A 74, 062508-1-20, 2006b.

Mereghetti, S., De Luca, A., Caraveo, P.A., Becker, W., Mignani, R., Bignami, G.F. Pulse phase variations of the X-ray spectral features in the radio-quiet neutron star 1E 1207–5209. ApJ 581, 1280–1285, 2002.

Mészáros, P. High-energy Radiation from Magnetized Neutron Stars. University of Chicago Press, Chicago, 1992.

Mészáros, P., Ventura, J. Vacuum polarization effects on radiative opacities in a strong magnetic field. Phys. Rev. D 19, 3565–3575, 1979.

Miller, M.C. Model atmospheres for neutron stars. MNRAS 255, 129–145, 1992.

Mori, K., Hailey, C.J. Atomic calculation for the atmospheres of strongly magnetized neutron stars. ApJ 564, 914–929, 2002.

Mori, K., Hailey, C.J. Detailed atmosphere modeling for the neutron star 1E 1207.4–5209: evidence of oxygen/neon atmosphere. ApJ 648, 1139–1155, 2006.

Mori, K., Ho, W.C.G. Modelling mid-Z element atmospheres for strongly magnetized neutron stars. MNRAS 377, 905–919, 2007.

Mori, K., Chonko, J.C., Hailey, C.J. Detailed spectral analysis of the 260 ks XMM-Newton data of 1E 1207.4–5209 and significance of a 2.1 kev absorption feature. ApJ 631, 1082–1093, 2005.

Morii, M., Sato, R., Kataoka, J., Kawai, N. Chandra observation of the anomalous X-ray pulsar 1E 1841–045. PASJ 55, L45–L48, 2003.

Motch, C., Zavlin, V.E., Haberl, F. Proper motion and energy distribution of the isolated neutron star RX J0720.4–3125. A&A 408, 323–330, 2003.

Özel, F. Surface emission properties of strongly magnetic neutron stars. ApJ 563, 276–288, 2001.

Patel, S.K. et al. Chandra observations of the anomalous X-ray pulsar 1E 2259+586. ApJL 563, L45–L48, 2001.

Patel, S.K. et al. Chandra observations of the anomalous X-ray pulsar 4U 0142+61. ApJ 587, 367–372, 2003.

Pavlov, G.G., Gnedin, Yu.N. Vacuum polarization by a magnetic field and its astrophysical manifestations. Sov. Sci. Rev. E 3, 197, 1984.

Pavlov, G.G., Shibanov, Yu.A. Influence of vacuum polarization by a magnetic field on the propagation of electromagnetic waves in a plasma. Sov. Phys. JETP 49, 741–757, 1979.

Pavlov, G.G., Shibanov, Yu.A., Ventura, J., Zavlin, V.E. Model atmospheres and radiation of magnetic neutron stars: anisotropic thermal emission. A&A 289, 837–845, 1994.

Pavlov, G.G., Shibanov, Yu.A., Zavlin, V.E., Meyer, R.D. Neutron star atmospheres, in: Alpar, M.A., Kiziloğlu, Ü., van Paradijs, J. (Eds.), Lives of the Neutron Stars. Kluwer, Boston, pp. 71–90, 1995.

Pavlov, G.G., Zavlin, V.E., Trümper, J., Neuhäuser, R. Multiwavelength observations of isolated neutron stars as a tool to probe the properties of their surfaces. ApJL 472, L33–L36, 1996.

Pavlov, G.G., Zavlin, V.E., Sanwal, D. Thermal radiation from neutron stars: Chandra results, in: Becker, W., Lesch, H., Trümper, J. (Eds.), Proceedings of the 270 WE-Heraeus Seminar on Neutron Stars, Pulsars, and Supernova Remnants (MPE Rep. 278; Garching: MPI), pp.273–286, 2002.

Pérez-Azorín, J.F., Miralles, J.A., Pons, J.A. Thermal radiation from magnetic neutron star surfaces. A&A 433, 275–283, 2005.

Pons, J.A., Walter, F.M., Lattimer, J.M., Prakash, M., Neuhäuser, R., An, P. Toward a mass and radius determination of the nearby isolated neutron star RX J185635–3754. ApJ 564, 981–1006, 2002.

Potekhin, A.Y., Chabrier, G. Equation of state and opacities for hydrogen atmospheres of neutron stars with strong magnetic fields. ApJ 585, 955–974, 2003.

Potekhin, A.Y., Chabrier, G. Equation of state and opacities for hydrogen atmospheres of magnetars. ApJ 600, 317–323, 2004.

Potekhin, A.Y., Chabrier, G., Shibanov, Yu.A. Partially ionized hydrogen plasma in strong magnetic fields. Phys. Rev. E 60, 2193–2208, 1999.

Potekhin, A.Y., Lai, D., Chabrier, G., Ho, W.C.G. Electromagnetic polarization in partially ionized plasmas with strong magnetic fields and neutron star atmosphere models. ApJ 612, 1034–1043, 2004.

Rajagopal, M., Romani, R.W. Model atmospheres for low-field neutron stars. ApJ 461, 327–333, 1996.

Rajagopal, M., Romani, R.W., Miller, M.C. Magnetized iron atmospheres for neutron stars. ApJ 479, 347–356, 1997.

Ransom, S.M., Gaensler, B.M., Slane, P.O. Deep search for pulsations from the nearby isolated neutron star RX J1856.5–3754. ApJL 570, L75–L78, 2002.

Romani, R.W. Model atmospheres for cooling neutron stars. ApJ 313, 718–726, 1987.

Sanwal, D., Pavlov, G.G., Zavlin, V.E., Teter, M.A. Discovery of absorption features in the X-ray spectrum of an isolated neutron star. ApJL 574, L61–L64, 2002.

Schwope, A.D., Hambaryan, V., Haberl, F., Motch, C. Pulsed X-ray light curves of the isolated neutron star RBS1223. A&A 441, 597–604, 2005.

Shibanov, Yu.A., Zavlin, V.E., Pavlov, G.G., Ventura, J. Model atmospheres and radiation of magnetic neutron stars – I. The fully ionized case. A&A 266, 313–320, 1992.

Thompson, C., Beloborodov, A.M. High-energy emission from magnetars. ApJ 634, 565–569, 2005.

Tiengo, A., Mereghetti, S. XMM-Newton discovery of 7 s pulsations in the isolated neutron star RX J1856.5–3754. ApJL 657, L101–L104, 2007.

Tiengo, A., Goehler, E., Staubert, R., Mereghetti, S. Anomalous X-ray pulsar 1E 1048.1–5937: phase resolved spectroscopy with the XMM-Newton satellite. A&A 383, 182–187, 2002.

Trümper, J.E., Burwitz, V., Haberl, F., Zavlin, V.E. The Puzzles of RX J1856.5–3754: neutron star or quark star? Proc. Suppl. Nucl. Phys. B 132, 560–565, 2004.

Tsai, Y.-S. Pair production and bremsstrahlung of charged leptons. Rev. Mod. Phys. 46, 815–851, 1974.

Tsai, W.Y., Erber, T. Propagation of photons in homogeneous magnetic fields: index of refraction. Phys. Rev. D 12, 1132–1137, 1975.

Turbiner, A.V., Vieyra, López Hydrogenic molecular atmosphere of a neutron star. Mod. Phys. Lett. A 19, 1919–1923, 2004.

Turolla, R., Zane, S., Drake, J.J. Bare quark stars or naked neutron stars? the case of RX J1856.5–3754. ApJ 603, 265–282, 2004.

van Adelsberg, M., Lai, D. Atmosphere models of magnetized neutron stars: QED effects, radiation spectra and polarization signals. MNRAS 373, 1495–1522, 2006.

van Adelsberg, M., Lai, D., Potekhin, A.Y., Arras, P. Radiation from condensed surface of magnetic neutron stars. ApJ 628, 902–913, 2005.

van Kerkwijk, M.H., Kulkarni, S.R. Optical spectroscopy and photometry of the neutron star RX J1856.5–3754. A&A 378, 986–995, 2001.

van Kerkwijk, M.H., Kaplan, D.L., Durant, M., Kulkarni, S.R., Paerels, F. Strong, broad absorption feature in the X-ray spectrum of the nearby neutron star RX J1605.3 + 3249. ApJ 608, 432–443, 2004.

Ventura, J., Nagel, W., Mészáros, P. Possible vacuum signature in the spectra of X-ray pulsars. ApJL 233, L125–L128, 1979.

Walter, F.M., Lattimer, J.M. A revised parallax and its implications for RX J185635–3754. ApJL 576, L145–L148, 2002.

Zane, S., Turolla, R., Treves, A. Magnetized atmospheres around neutron stars accreting at low rates. ApJ 537, 387–395, 2000.

Zane, S., Turolla, R., Stella, L., Treves, A. Proton cyclotron features in thermal spectra of ultramagnetized neutron stars. ApJ 560, 384–389, 2001.

Zane, S., Cropper, M., Turolla, R., Zampieri, L., Chieregato, M., Drake, J.J., Treves, A. XMM-Newton detection of pulsations and a spectral feature in the X-ray emission of the isolated neutron star 1RXS J214303.7+065419/RBS 1774. ApJ 627, 397–403, 2005.

Zavlin, V.E., Pavlov, G.G. Modeling neutron star atmospheres, in: Becker, W., Lesch, H., Trümper, J. (Eds.), Proceedings of the 270 WE-Heraeus Seminar on Neutron Stars, Pulsars, and Supernova Remnants (MPE Rep. 278; Garching: MPI), pp.263–272, 2002.

Zavlin, V.E., Pavlov, G.G., Shibanov, Yu.A. Model neutron star atmospheres with low magnetic fields. I. Atmospheres in radiative equilibrium. A&A 315, 141–152, 1996.